

In Vivo Evaluation of White Matter Integrity and Anterograde Transport in Visual System After Excitotoxic Retinal Injury With Multimodal MRI and OCT

Leon C. Ho,¹⁻³ Bo Wang,^{2,4,5} Ian P. Conner,^{2,4,5} Yolandi van der Merwe,^{1,2,4-6} Richard A. Bilonick,^{2,4,7} Seong-Gi Kim,^{1,4,6,8-10} Ed X. Wu,³ Ian A. Sigal,^{2,4-6} Gadi Wollstein,^{2,5} Joel S. Schuman,^{2,4-6,10,11} and Kevin C. Chan^{1,2,4-6,10}

¹NeuroImaging Laboratory, University of Pittsburgh, Pittsburgh, Pennsylvania, United States

²UPMC Eye Center, Ophthalmology and Visual Science Research Center, Department of Ophthalmology, School of Medicine, University of Pittsburgh, Pittsburgh, Pennsylvania, United States

³Department of Electrical and Electronic Engineering, The University of Hong Kong, Pokfulam, Hong Kong, China

⁴Department of Bioengineering, Swanson School of Engineering, University of Pittsburgh, Pittsburgh, Pennsylvania, United States

⁵Louis J. Fox Center for Vision Restoration, University of Pittsburgh, Pittsburgh, Pennsylvania, United States

⁶McGowan Institute for Regenerative Medicine, University of Pittsburgh, Pittsburgh, Pennsylvania, United States

⁷Department of Biostatistics, Graduate School of Public Health, University of Pittsburgh, Pittsburgh, Pennsylvania, United States

⁸Departments of Biological Sciences and Biomedical Engineering, Sungkyunkwan University, Suwon, Korea

⁹Center for Neuroscience Imaging Research, Institute for Basic Science, Sungkyunkwan University, Suwon, Korea

¹⁰Center for the Neural Basis of Cognition, University of Pittsburgh and Carnegie Mellon University, Pittsburgh, Pennsylvania, United States

¹¹Clinical and Translational Science Institute, University of Pittsburgh, Pittsburgh, Pennsylvania, United States

Correspondence: Kevin C. Chan, Departments of Ophthalmology and Bioengineering, University of Pittsburgh, Pittsburgh, PA, USA; chuenwing.chan@fulbrightmail.org.

LCH and BW contributed equally to the work presented here and should therefore be regarded as equivalent authors.

Submitted: August 26, 2014

Accepted: April 20, 2015

Citation: Ho LC, Wang B, Conner IP, et al. In vivo evaluation of white matter integrity and anterograde transport in visual system after excitotoxic retinal injury with multimodal MRI and OCT. *Invest Ophthalmol Vis Sci*. 2015;56:3788-3800. DOI:10.1167/iov.14-15552

PURPOSE. Excitotoxicity has been linked to the pathogenesis of ocular diseases and injuries and may involve early degeneration of both anterior and posterior visual pathways. However, their spatiotemporal relationships remain unclear. We hypothesized that the effects of excitotoxic retinal injury (ERI) on the visual system can be revealed in vivo by diffusion tensor magnetic resonance imaging (DTI), manganese-enhanced magnetic resonance imaging (MRI), and optical coherence tomography (OCT).

METHODS. Diffusion tensor MRI was performed at 9.4 Tesla to monitor white matter integrity changes after unilateral N-methyl-D-aspartate (NMDA)-induced ERI in six Sprague-Dawley rats and six C57BL/6J mice. Additionally, four rats and four mice were intravitreally injected with saline to compare with NMDA-injected animals. Optical coherence tomography of the retina and manganese-enhanced MRI of anterograde transport were evaluated and correlated with DTI parameters.

RESULTS. In the rat optic nerve, the largest axial diffusivity decrease and radial diffusivity increase occurred within the first 3 and 7 days post ERI, respectively, suggestive of early axonal degeneration and delayed demyelination. The optic tract showed smaller directional diffusivity changes and weaker DTI correlations with retinal thickness compared with optic nerve, indicative of anterograde degeneration. The splenium of corpus callosum was also reorganized at 4 weeks post ERI. The DTI profiles appeared comparable between rat and mouse models. Furthermore, the NMDA-injured visual pathway showed reduced anterograde manganese transport, which correlated with diffusivity changes along but not perpendicular to optic nerve.

CONCLUSIONS. Diffusion tensor MRI, manganese-enhanced MRI, and OCT provided an in vivo model system for characterizing the spatiotemporal changes in white matter integrity, the eye-brain relationships and structural-physiological relationships in the visual system after ERI.

Keywords: glutamate excitotoxicity, optic neuropathy, corpus callosum, magnetic resonance imaging, optical coherence tomography

Excitotoxicity has been linked to the pathogenesis of several ocular diseases and injuries such as retinal ischemia,¹⁻⁵ traumatic injury,^{6,7} glaucoma,⁸⁻¹¹ and diabetic retinopathy.^{12,13} In the retina, the retinal ganglion cells preferentially express N-methyl-D-aspartate (NMDA)-type glutamate receptors and are believed to play a major role in glutamate excitotoxic retinal

injury.^{14,15} While the cell bodies in the retina are commonly regarded as the primary site of insult, recent studies have suggested the early involvement of white matter degeneration in the posterior visual pathway after glutamate excitotoxicity in the eye.¹⁶⁻¹⁹ Nevertheless, because of limited noninvasive techniques available for assessing the visual pathways, the

spatiotemporal patterns of neurodegenerative events in the visual system and their relationships with excitotoxic retinal injury in the eye are not fully elucidated. This in part hinders the development of effective strategies for disease monitoring and treatment.

Magnetic resonance imaging (MRI) allows noninvasive, longitudinal, and multiparametric assessments of the visual system without depth limitation.^{20–25} Although there were existing MR reports assessing the effects of NMDA-induced excitotoxicity in developing and adult brain tissues,^{26,27} most of the neuropathy models employed did not differentiate clearly the locations of the primary site of insult or the initial events in white matter degeneration. In addition, the early MRI studies assessing visual system injury^{28,29} mainly used the conventional anatomical T2-weighted imaging or diffusion weighted imaging techniques at low magnetic field strengths with relatively limited sensitivity and specificity to characterize the underlying pathophysiological events. In this study, we employed the advanced MR techniques, namely diffusion tensor MRI (DTI) and manganese-enhanced MRI (MEMRI) at a high magnetic field strength, in combination with spectral-domain optical coherence tomography (OCT), with an aim to develop an in vivo model system for characterizing the spatiotemporal patterns of white matter integrity changes in the visual system and their relations to retinal integrity after glutamate excitotoxicity in the eye. Diffusion tensor MRI has been recently shown to reveal white matter integrity in normal, developing and diseased visual systems in rodent models under high magnetic field strengths.^{30–35} In particular, the measurements of water diffusion parallel and perpendicular to the nerve fibers have been suggested to be sensitive to axonal and myelin integrity respectively.^{31,36} Since intravitreal injection of NMDA has been commonly used as an experimental model to induce glutamate excitotoxic retinal ganglion cell death,^{37,38} in this study, we quantified the spatiotemporal DTI profiles in the rodent visual system with a 9.4 Tesla MRI scanner after NMDA-induced excitotoxic retinal injury. In addition, DTI results were compared with OCT measurement of the thickness of the retina and MEMRI of the anterograde transport along the visual pathway, in order to determine the eye–brain relationships and to correlate between structural and physiological characteristics in the injured visual system. As the retinal ganglion cells and the sites of toxic insult after intravitreal NMDA injection in the eye are physically isolated from the axons beyond the eye in the brain's visual system, our MRI and OCT studies in this NMDA model of retinal injury are well suited for providing information about the effects of excitotoxic perikaryal injury on white matter integrity changes in both ocular diseases and other neuropathies. Our cross-sectional and longitudinal results from these in vivo multidisciplinary ophthalmic imaging techniques may allow better monitoring of the disease progression in the visual system, and provide a platform for assessing treatment effects on both the eye and the visual pathway in future studies.

MATERIALS AND METHODS

Animal Preparation

All animal experiments were performed in accordance with the ARVO Statement for the Use of Animals in Ophthalmic and Vision Research and protocols reviewed and approved by the University of Pittsburgh's Institutional Animal Care and Use Committee. Ten adult Sprague-Dawley rats and 10 adult C57BL/6J mice were divided into four groups to evaluate the effects of NMDA-induced glutamate excitotoxicity in the eye on the visual system. In Group 1, six adult rats were first anesthetized by

inhaling a mixture of air and isoflurane (3% for induction and 1.25% for maintenance). Proparacaine (Bausch & Lomb, Inc., Rochester, NY, USA) was topically administered to anesthetize the surface of the eye, followed by intravitreal injection of 5 μ L 40 mM NMDA (Thermo Fisher Scientific, Inc., Waltham, MA, USA) into the right eye using a 33-G microsyringe (Hamilton Co., Reno, NV, USA) to induce glutamate excitotoxicity to the retina. In Group 2, the same experimental procedures were performed to the four remaining rats, except that 5 μ L saline solution (0.9% sodium chloride; Baxter International, Inc., Deerfield, IL, USA) instead of NMDA solution was intravitreally injected to the right eye. Diffusion tensor MRI was performed to each rat at 3, 7, 14, and 28 days after NMDA or saline injection, while OCT was performed to four rats randomly selected from Group 1 and to all four rats in Group 2 after DTI at the final time point. For Group 3, 1 μ L 40 mM NMDA was intravitreally injected to the right eye of six adult mice under the same experimental settings as the rat model. For Group 4, 1 μ L saline solution was intravitreally injected to the right eye of the remaining 4 mice. Diffusion tensor MRI was performed to each mouse at 7 ($n = 6$ for NMDA group; $n = 4$ for saline group) and 70 days ($n = 4$ for NMDA group; $n = 3$ for saline group due to loss of one animal between 7 and 70 days) after NMDA or saline injection. In addition, each mouse was intravitreally injected with 0.5 μ L 100 mM manganese chloride (MnCl₂) solution into both eyes after DTI at 7 days after NMDA or saline injection, and T1-weighted MEMRI was performed before and at 8 hours after Mn injection. A saline syringe phantom was placed next to the mouse head for T1-weighted MR signal normalization to counter for system instability between imaging sessions.

The current NMDA doses were chosen with reference to recent studies investigating NMDA-induced injury in rodent retina.^{37,38} Since the main purpose of this study was to examine the effects of NMDA-induced glutamate excitotoxicity in the eye on the visual pathway via in vivo imaging, whereas intravitreal NMDA injection led to excitotoxic retinal injury in a dose-dependent manner,^{37,39,40} we induced glutamate excitotoxicity at a relatively high NMDA dose to maximize retinal damage while minimizing the number of animals required to first prove the concept that DTI, MEMRI, and OCT could detect the spatiotemporal changes in the white matter integrity and their relations to retinal integrity after NMDA-induced excitotoxicity in the eye.

DTI and MEMRI

All MRI experiments were performed using a 9.4-Tesla/31-cm Varian/Agilent horizontal bore scanner (Santa Clara, CA, USA) with a volume transmit coil and a surface receive coil for rats and a volume transmit and receive coil for mice. Animals were anesthetized with a mixture of air and isoflurane (3% for induction and 1.5% for maintenance) and were kept warm under circulating water during MRI experiments. To ensure reproducible slice orientation and positioning, scout T2-weighted images were first acquired in the coronal, transverse, and sagittal planes with a spin-echo pulse sequence.²³ Diffusion tensor MRI slices were oriented orthogonal to the prechiasmatic optic nerves and were acquired using a fast spin-echo sequence, with 12 diffusion gradient directions at $b = 1.0$ ms/ μ m² and two $b = 0$ ms/ μ m² (b_0). Other imaging parameters included: repetition time/echo time = 2300/27.8 ms; echo train length = 8; duration of diffusion gradient pulses (δ)/time between diffusion gradient pulses (Δ) = 5/17 ms; number of averages = 4; field of view = 26 \times 26 (rat) and 20 \times 20 mm² (mouse); in-plane resolution = 102 \times 102 (rat) and 78 \times 78 μ m² (mouse); slice thickness = 1 (rat) and 0.5 mm (mouse). Manganese-enhanced MRI was acquired using a T1-weighted fast spin-echo sequence, with the same geometric parameters,

Diffusion Tensor MRI of Rat Visual Pathway

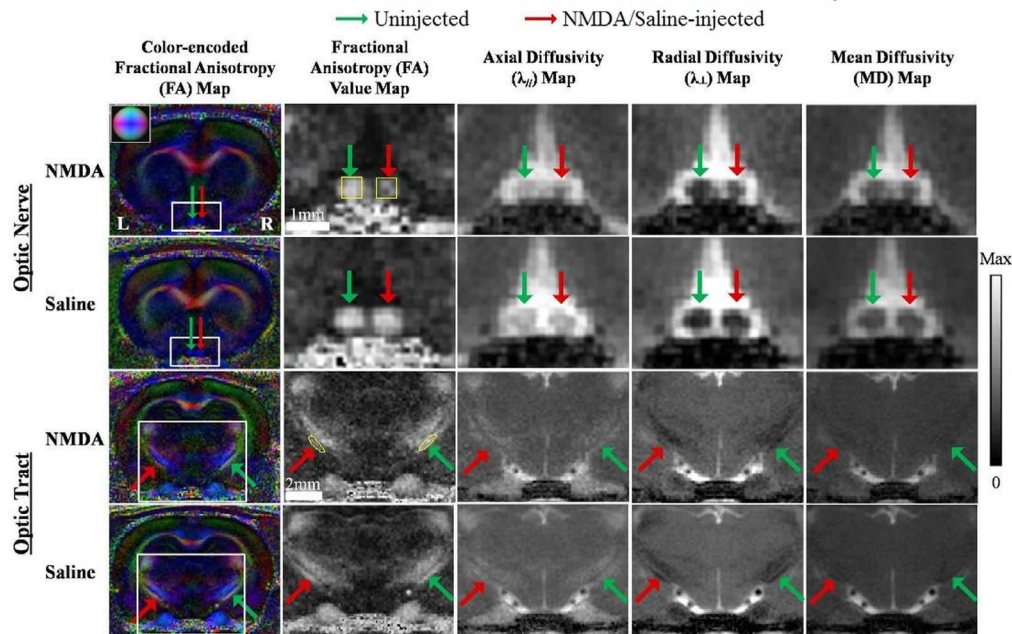


FIGURE 1. Representative DTI parametric maps of the rat brain at the levels of the prechiasmatic optic nerve (*top 2 rows*) and optic tract (*bottom 2 rows*) at 4 weeks after NMDA (*first and third rows*) or saline injection (*second and fourth rows*) to the right eye. The *leftmost column* shows the whole-brain color-encoded FA directionality maps, whereas the FA value maps, and axial diffusivity ($\lambda_{//}$), radial diffusivity (λ_{\perp}), and mean diffusivity (MD) maps on the *right columns* are enlarged from the *white boxes* in the whole-brain color-encoded FA maps. *Red arrows* indicate the visual pathway projected from the injected right eye. *Green arrows* indicate the visual pathway projected from the uninjected left eye. The right optic nerve and left optic tract projected from the NMDA-injected right eye showed lower FA and $\lambda_{//}$, and higher λ_{\perp} when compared with the contralateral visual pathway projected from the uninjected left eye. No apparent change in any DTI parameters was observed between the left and right visual pathways after saline injection to the right eye. The regions of interest in the optic nerves and optic tracts for DTI quantitation are outlined in *yellow* (color representations for the principal diffusion directions in the color-encoded FA maps: *Blue*, caudal-rostral; *red*, left-right; *green*, dorsal-ventral; *grayscale bar* indicates the range of values displayed in the DTI parametric maps. The maximum values for FA, $\lambda_{//}$, λ_{\perp} and MD maps are 1.0, 3.0, 2.0, and $3.0 \mu\text{m}^2/\text{ms}$, respectively).

repetition time/echo time = 1060/9.35 ms and echo train length = 4.

Optical Coherence Tomography

Prior to OCT imaging, the rats were anesthetized with an intraperitoneal injection of ketamine (Butler Schein, Dublin, OH, USA) and xylazine (Lloyd Laboratories, Shenandoah, IA, USA). A thin glass coverslip and hydroxypropyl methylcellulose (HUB Pharmaceuticals, Rancho Cucamonga, CA, USA) was applied to neutralize the corneal curvature and keep the cornea hydrated. The scans were acquired within 15 minutes of anesthesia to limit the effects of lenticular opacities. The spectral-domain OCT device (Bioptigen, Inc., Research Triangle Park, NC, USA) is equipped with a wide-bandwidth light source centered on 870 nm (Superlum Ltd., Dublin, Ireland), with a theoretical axial resolution of $1.3 \mu\text{m}$ in tissue. A $2.5 \times 2.5 \times 2 \text{ mm}^3$ ($512 \times 512 \times 1024$) volume centered on the optic nerve head was taken on both eyes.

Data Analysis

For DTI, coregistration between nondiffusion-weighted b_0 images and diffusion-weighted images was performed using SPM8 (Wellcome Department of Imaging Neuroscience, University College, London, UK). Using DTIStudio v3.02 (Johns Hopkins University, Baltimore, MD, USA), 3×3 diffusion tensors were fitted on a pixel-by-pixel basis from the nondiffusion-weighted b_0 images and the diffusion-weighted images. The eigenvectors and eigenvalues of the

diffusion tensors were derived to compute the DTI parametric maps including fractional anisotropy (FA) directionality color map, FA value map, and axial diffusivity ($\lambda_{//}$), radial diffusivity (λ_{\perp}), and mean diffusivity (MD) maps. Regions of interest were drawn manually using ImageJ v1.47 software (<http://imagej.nih.gov/ij/>; provided in the public domain by the National Institutes of Health, Bethesda, MD, USA) on the prechiasmatic optic nerves at Bregma 1.5 mm, the optic tracts at Bregma -3.5 mm, and the splenium of corpus callosum at Bregma -5.04 mm for rats based on the FA directionality map, FA value map, $\lambda_{//}$ and λ_{\perp} maps, and the rat brain atlas.⁴¹ Regions of interest were also drawn on the mouse prechiasmatic optic nerves at Bregma 1.0 mm and the optic tracts at Bregma -1.8 mm based on the FA directionality map, FA value map, $\lambda_{//}$ and λ_{\perp} maps and the mouse brain atlas.⁴²

For OCT, the volumes centered on the optic nerve head on both eyes were automatically segmented using a custom software⁴³ to determine the internal limiting membrane (ILM) and retinal pigment epithelium (RPE). The center of the optic nerve head was manually delineated. Total retinal thickness, or the distance between the ILM and RPE, was determined along a sampling band with radius 0.39 to 0.49 mm centered on the optic nerve head.

For MEMRI, regions of interest were drawn manually using ImageJ on the optic nerves at Bregma 1.0 mm, the lateral geniculate nuclei at Bregma -3.0 mm and the superior colliculi at Bregma -4.0 mm based on T1-weighted anatomical images and the mouse brain atlas.⁴² T1-weighted signal intensities pre- and post Mn injection were extracted and normalized to the signal intensity of the nearby saline syringe phantom.

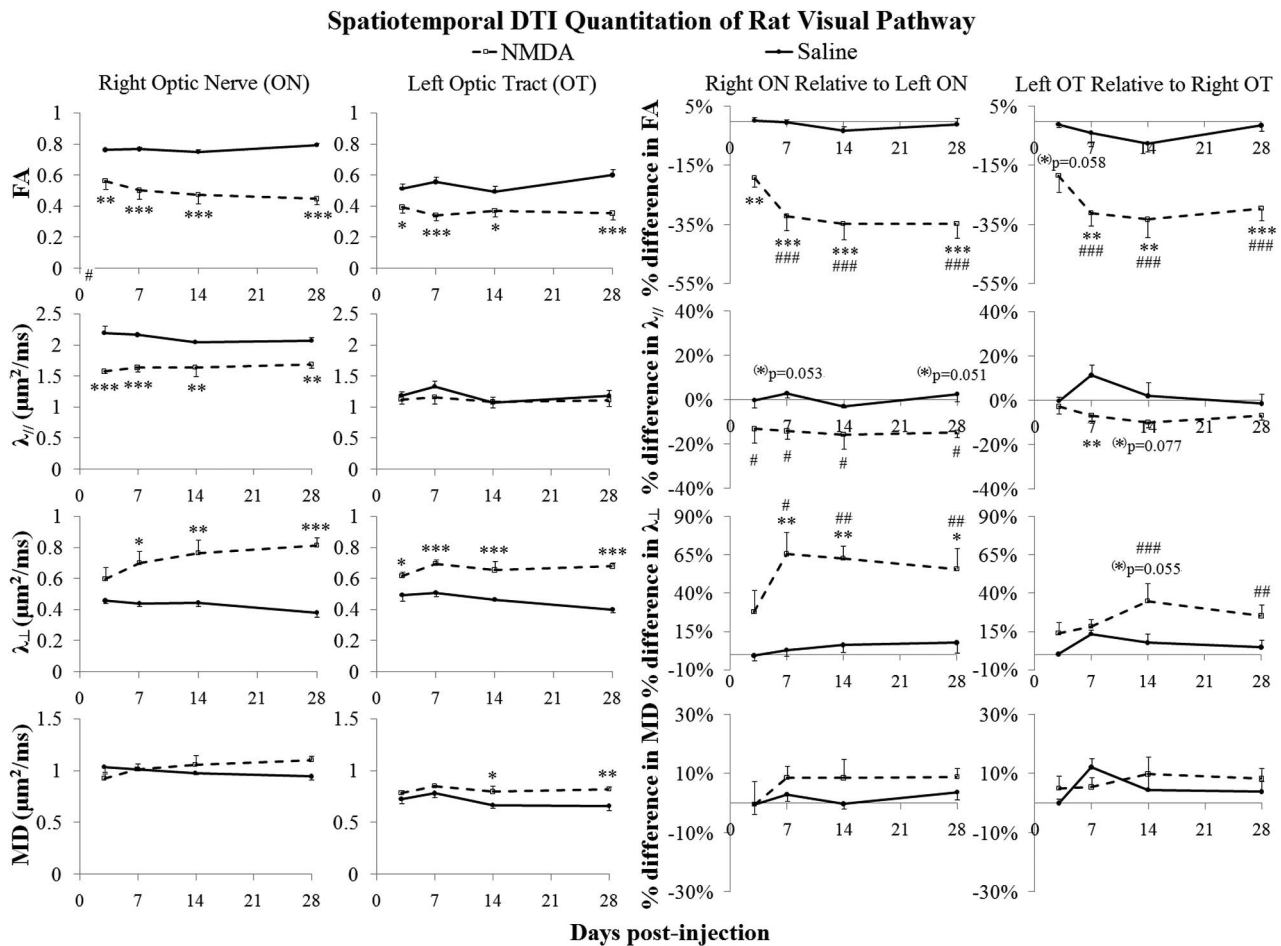


FIGURE 2. Spatiotemporal DTI quantitation (mean \pm SEM) in the right optic nerve (*first column*) and left optic tract (*second column*) and the percentage DTI difference (mean \pm SEM) in the right optic nerve (*third column*) or left optic tract (*fourth column*) relative to the contralateral visual pathway at 3 to 28 days after NMDA or saline injection to the right eye in rats (Bonferroni's multiple comparisons tests between NMDA and saline groups, * $P < 0.05$, ** $P < 0.01$, *** $P < 0.001$; between left and right visual pathways in the NMDA group, # $P < 0.05$, ## $P < 0.01$, ### $P < 0.001$). The right optic nerve projected from the NMDA-injected eye showed significantly lower FA and axial diffusivity ($\lambda_{//}$), and higher radial diffusivity (λ_{\perp}) compared with the saline group. The left optic tract projected from the NMDA-injected eye generally showed smaller DTI changes than the right optic nerve of the same group, or the left optic tract from the saline group. No apparent difference was observed between the left and right visual pathways in the saline group.

Statistical Analysis

As previous studies suggested that unilateral injury to one eye may affect the contralateral eye,⁴⁴⁻⁴⁷ whereas in adult rodents, more than 90% of the optic nerve fibers decussate at the optic chiasm to the contralateral optic tract,⁴⁸ in this study, DTI, MEMRI, and OCT measurements were first compared between the visual pathways projected from the NMDA- and saline-injected eyes (i.e., right retina, right optic nerve, left optic tract, left lateral geniculate nucleus, and left superior colliculus) and in the splenium of corpus callosum using ANOVA followed by post hoc Bonferroni's multiple comparisons tests by GraphPad Prism v5.00 (GraphPad Software, Inc., La Jolla, CA, USA). The differences between left and right visual pathways were also evaluated and compared between NMDA and saline groups using ANOVA and post hoc Bonferroni's tests. In addition, random intercept mixed-effects models were included to determine the relationships between DTI and OCT data, and between DTI and MEMRI data. For the analyses of DTI and OCT data, the random intercept mixed-effects model was structured to assess the effect of total retinal thickness in both eyes and NMDA-induced injury on each DTI parameter

(FA, $\lambda_{//}$, λ_{\perp} , and MD), with rat as the random effect. For the analyses of DTI and Mn data, the random intercept mixed-effects model was structured to assess the effect of each DTI parameter (FA, $\lambda_{//}$, λ_{\perp} , and MD) in the optic nerve and NMDA-induced injury on MEMRI of both left and right visual pathways, with mouse as the random effect. The inter-eye dependency was accounted for when evaluating the models. The slopes among DTI, MEMRI, and OCT parameters in the models were also estimated. Data were presented as mean \pm SEM unless otherwise specified. Results were considered statistically significant when P was less than 0.05.

RESULTS

Spatiotemporal DTI Profiles of Rat Optic Nerve and Optic Tract Integrity After Unilateral NMDA-Induced Retinal Injury or Intravitreal Saline Injection

Figure 1 shows the qualitative comparisons of white matter integrity along the rat visual pathways at 1 month after

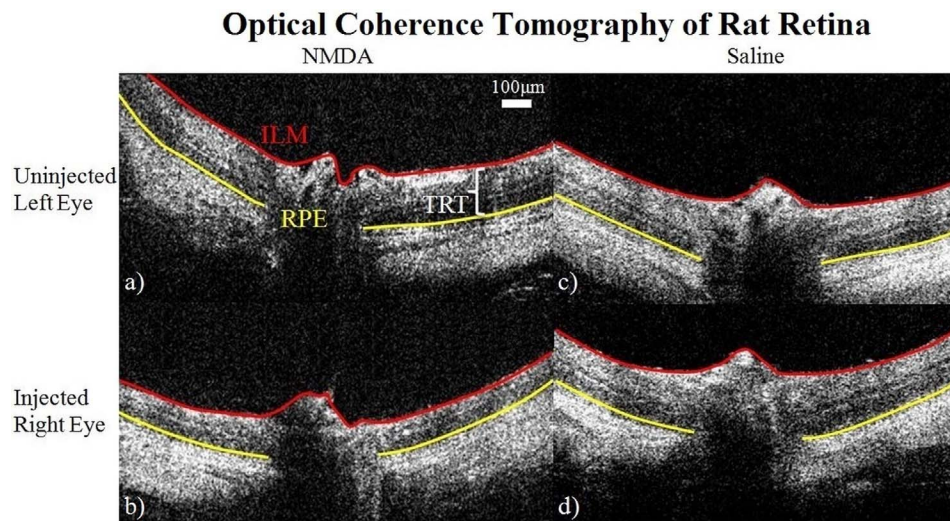


FIGURE 3. Cross-sectional images from OCT of the rat retina in the uninjected left eye (a, c) and injected right eye (b, d) at 1 month after intravitreal NMDA (left column) or saline injection (right column). The internal limiting membrane (ILM; white) and retinal pigment epithelium (RPE; red) were segmented in order to determine the total retinal thickness (TRT). Retinal thinning was observed in the NMDA-injected right eye (b) compared with the saline-injected right eye (d) or the uninjected left eye of either NMDA (a) or saline group (c).

NMDA-induced glutamate excitotoxicity or saline injection in the right eye in Groups 1 and 2. As shown in the DTI parametric maps, the right optic nerve and left optic tract projected from the NMDA-injected right eye showed lower FA, lower $\lambda_{//}$, and higher λ_{\perp} compared with the left optic nerve and right optic tract. No apparent difference in any DTI parameters was observed between left and right visual pathways after saline injection to the right eye. Diffusion tensor MRI quantitation in Figure 2 reveals the progressive changes in optic nerve and optic tract integrity from 3 to 28 days after NMDA-induced retinal injury or saline injection. When comparing the right optic nerve between NMDA and saline groups, significantly lower FA and $\lambda_{//}$ were detected in the NMDA group as early as 3 days after NMDA injection, whereas significantly higher λ_{\perp} occurred later at 7 days and onward after NMDA injection. The left optic tract projected from the injected eye showed generally smaller DTI differences between NMDA and saline groups when compared with the right optic nerve. The percentage DTI differences between visual pathways projected from the injected and uninjected eyes of the same groups were also quantified in Figure 2. The spatiotemporal patterns of the DTI percentage differences between left and right visual pathways in the NMDA group appeared comparable to the DTI differences in the right optic nerve or left optic tract between NMDA and saline groups. In addition, continuously increasing FA decrease and λ_{\perp} increase were apparent in the NMDA group within the first week post ERI, whereas $\lambda_{//}$ decrease in NMDA group remained relatively constant throughout the experimental period from 3 to 28 days post ERI. No significant DTI difference was observed between visual pathways projected from the injected and uninjected eyes of the saline group throughout the experimental period.

OCT of Retinal Thickness and Correlations With DTI of Visual Pathway Integrity

Figure 3 shows the representative OCT images of the rat retina in both eyes at approximately 1 month after NMDA or saline injection to the right eye. Significant retinal thinning was observed in the NMDA-injected right eye compared with the saline-injected right eye or the uninjected left eye of either

NMDA or saline group. Quantitatively, the mean total retinal thickness in the injected and uninjected eyes were comparable at 237.8 ± 27 and 231.6 ± 26 μm respectively in the saline group (Bonferroni's post hoc test, $P > 0.05$), and 174 ± 13 and 223 ± 16 μm , respectively, in the NMDA group (Bonferroni's post hoc test, $P < 0.001$), indicative of a significant reduction in total retinal thickness by 22% in the injected right eye relative to the uninjected left eye in the NMDA group. The total retinal thickness measured from OCT was compared with the DTI measurements in the optic nerve and optic tract with the random intercept mixed-effects model. As shown in Figure 4, correlation plots between retinal thickness and DTI parameters generally showed steeper slopes for the optic nerve than the optic tract. The total retinal thickness was found to be significantly and positively correlated with FA in both optic nerve and optic tract. It was also positively correlated with $\lambda_{//}$ in the optic tract and negatively correlated with λ_{\perp} in the optic nerve with statistical significance. The effects of NMDA-induced injury on total retinal thickness were also significantly correlated with the random intercept mixed-effects model.

DTI of White Matter Integrity in Splenium of Corpus Callosum

The splenium of corpus callosum in the NMDA group showed a significant increase in FA and $\lambda_{//}$ by 17.1% and 13.1%, respectively, at 4 weeks relative to 3 days after NMDA injection to the right eye (Fig. 5). None of the DTI parametric measurements in the saline group showed significant changes over the experimental period.

DTI of Visual Pathway Integrity and Correlations With MEMRI of Anterograde Transport in Mice

As shown in Figure 6, the NMDA mouse model in Group 3 showed comparable spatiotemporal DTI profiles to the rat model in Group 1. Specifically, significantly lower FA and $\lambda_{//}$ were observed in the right optic nerve and left optic tract projected from the NMDA-injected eye relative to the visual pathway projected from the saline-injected eye in Group 4 at 7 to 70 days post injection. No significant difference in any DTI parametric measurements was observed between visual

Relationships between OCT of Retina and DTI of Optic Nerve and Optic Tract

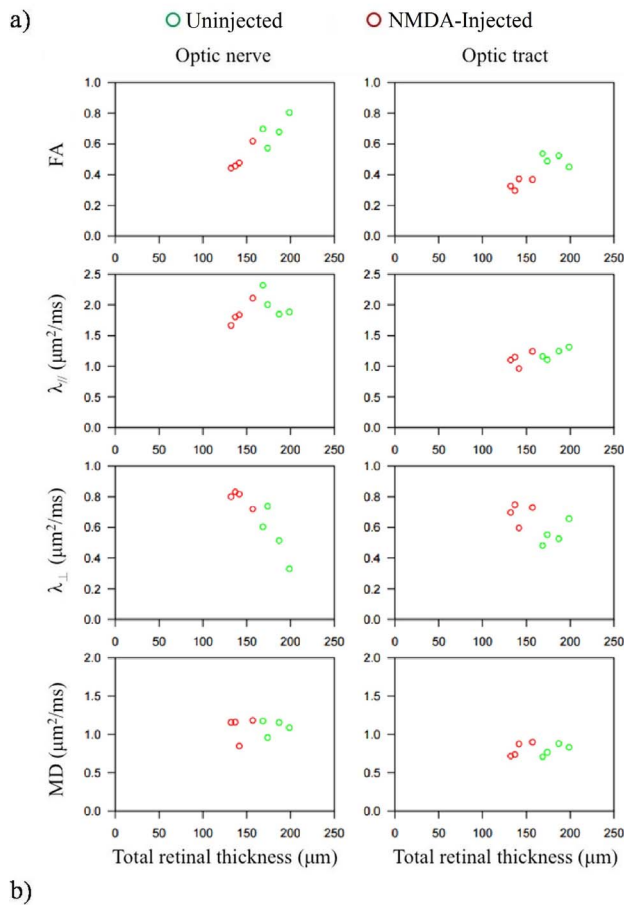


FIGURE 4. (a) Relationships between total retinal thickness in OCT (x-axis) and DTI parameters (y-axis) in the rat optic nerve (left column) and optic tract (right column) of both left and right visual pathways at 1 month after NMDA-induced glutamate excitotoxicity in the right eye. The data points for the visual pathways projected from the uninjected eye and the NMDA-injected eye are labeled in green and red, respectively. (b) The estimated slopes of DTI parameters in the optic nerve or optic tract against total retinal thickness ($P < 0.05$: estimated slopes are significantly different from 0). Fractional anisotropy and $\lambda_{||}$ generally showed positive correlations with total retinal thickness, whereas λ_{\perp} and MD generally showed negative correlations with TRT. The magnitudes of the slopes between DTI parameters and retinal thickness were larger in the optic nerve than optic tract.

pathways projected from the injected and uninjected eyes in the saline group throughout the experimental period.

In the T1-weighted MR images at 1 week after NMDA or saline injection to the right eye and 8 hours after binocular Mn injection (Fig. 7). The Mn enhancement along the visual pathway projected from the NMDA-injected eye was significantly weaker than that projected from the uninjected eye of the same group, or from the saline-injected eye. Using the random intercept mixed-effects model (Fig. 8), FA and $\lambda_{||}$ in the

optic nerve were significantly and positively correlated with Mn signal enhancement in the optic nerve, lateral geniculate nucleus and superior colliculus. No significant correlation was observed between λ_{\perp} in the optic nerve and Mn signal enhancement along the visual pathway.

DISCUSSION

In this study, we characterized quantitatively by in vivo DTI the effects of NMDA-induced glutamate excitotoxicity in the eye on the spatiotemporal profiles of white matter integrity in the brain's visual system. Our DTI findings of the early $\lambda_{||}$ decrease and delayed λ_{\perp} increase in the optic nerve within the experimental period may reflect different progression rates for several pathophysiological events known to occur in distal neural pathways such as early axonal injury and delayed demyelination. The stronger correlations between OCT of retinal loss and DTI of white matter integrity in the optic nerve than optic tract, and the late reorganization of the splenium of corpus callosum appeared consistent with the patterns of anterograde degeneration in the visual system after NMDA-induced excitotoxic retinal injury. In the NMDA mouse model, reduction of physiological anterograde transport of the active Mn tracer was observed along the injured visual pathway projected from the NMDA-injected eye. In addition, the strong preferential correlations of Mn enhancement with $\lambda_{||}$ and FA but not λ_{\perp} in the optic nerve suggested the potential linkage between anterograde Mn transport disruption and the compromise of microstructures that predominated water diffusion changes parallel to the optic nerve such as microtubule and neurofilament injuries. Taken together, our results demonstrated the capability of in vivo imaging markers to reveal the pathological events, the eye-brain relationships and structural-functional relationships in the brain's visual system after eye injury. These results are potentially important in offering a model system to assess treatment strategies to both the eye and the brain in future studies.

Previous histologic studies have suggested the spread of neuronal cell degeneration to the posterior visual pathway early after excitotoxic retinal injury.^{16,19,30} Our DTI findings indicated that these degenerative processes could be detected in vivo though indirectly by probing water diffusion properties noninvasively. Fractional anisotropy in DTI may reflect the directionality and overall integrity of the white matter. In the optic nerve, the continual FA decrease within the first 7 days after excitotoxic retinal injury appeared to be concurrent with ultrastructural findings revealed by ex vivo transmission electron tomography, whereby only parts of the neural components were injured at 3 days after injury, but almost all the optic nerve fibers were altered at 7 days after intravitreal NMDA injection at similar doses.¹⁶ On the other hand, the directional diffusivities $\lambda_{||}$ and λ_{\perp} have been reported to be sensitive to axonal and myelin integrity changes, respectively, in the white matter.^{30,31,49-52} Upon excitotoxic retinal injury at similar NMDA doses, axonal swelling, and loss of microtubules had been found in the distal optic nerve within 3 days after NMDA injection,¹⁶ with relative preservation of neurofilaments and myelin sheath. These phenomena appeared to restrict water diffusion preferentially along the optic nerve leading to the observed $\lambda_{||}$ decrease. As the degeneration progressed, almost all axonal microstructures were collapsed and demyelination was frequently seen in the optic nerve by 7 days after NMDA injection.¹⁶ Such patterns of disease progression may explain the delayed λ_{\perp} increase in the optic nerve at 7 days relative to early $\lambda_{||}$ decrease observed at 3 days after NMDA injection. Fractional anisotropy, $\lambda_{||}$, and λ_{\perp} may offer sensitive in vivo imaging markers to help monitor the progression rates

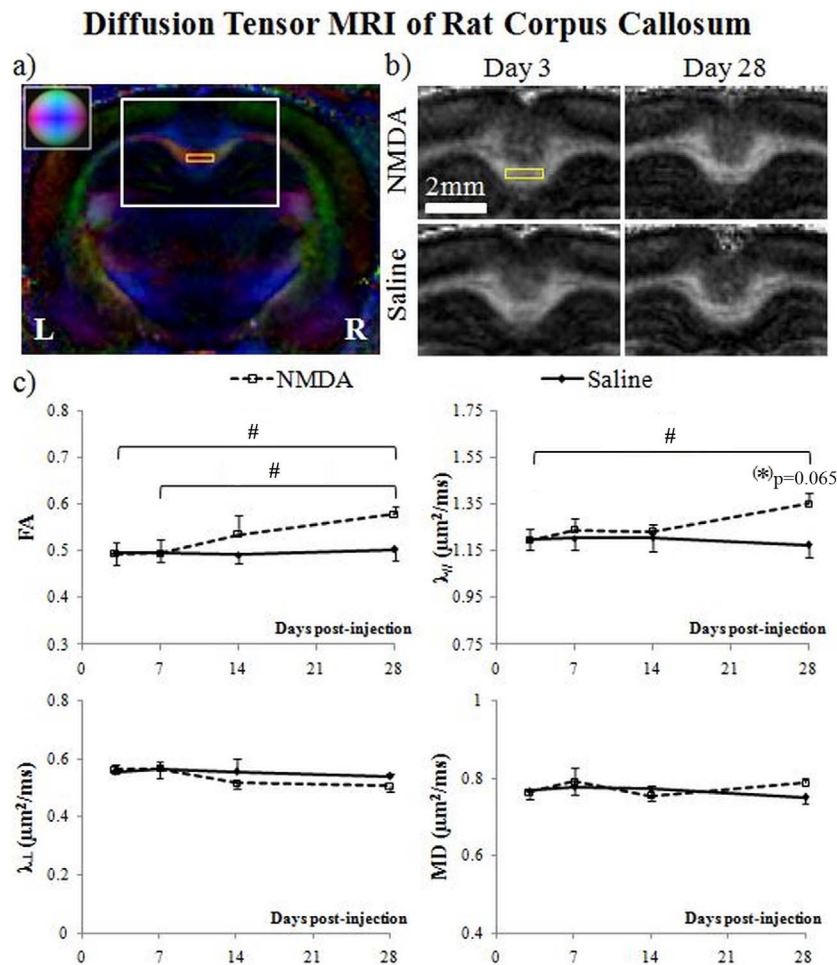


FIGURE 5. (a) Representative color-encoded FA maps of the rat brain at the level of the splenium of corpus callosum. (b) Representative FA value maps enlarged from the white box in (a) showing the splenium of corpus callosum at 3 and 28 days after NMDA or saline injection to the right eye. The region of interest for DTI quantitation of the splenium of corpus callosum is outlined in yellow. (c) Diffusion tensor MRI quantitation (mean \pm SEM) of the splenium of corpus callosum throughout the experimental period. Significant increases in FA and $\lambda_{//}$ were observed in the NMDA group at day 28 relative to day 3 post injection (Bonferroni's multiple comparisons tests across time, # $P < 0.05$; between NMDA and saline groups, * $P < 0.05$; color representations for the principal diffusion directions in the color-encoded FA maps: blue, caudal-rostral; red, left-right; green, dorsal-ventral).

for different pathological events in the optic nerve after glutamate excitotoxicity in the eye.

By comparing the DTI parametric changes between the optic nerve and optic tract, the directional diffusivities $\lambda_{//}$ and λ_{\perp} appeared to be more sensitive markers than FA and MD in differentiating the spatial relationships of neurodegeneration in the brain's visual system after excitotoxic retinal injury. The relatively larger $\lambda_{//}$ and λ_{\perp} changes in the optic nerve than the optic tract indicated that the compromise in white matter integrity was more pronounced in the proximal than distal visual pathway, likely as a result of the involvement of Wallerian-like anterograde degeneration in the brain's visual system.¹⁶ Such patterns of degenerative processes were further supported by the stronger eye-brain relationships between OCT's retinal thickness and DTI parameters in the optic nerve compared with the optic tract. The retinal thinning detected in this study apparently reflected the NMDA-induced damages to the ganglion cell and inner plexiform layers in the ganglion cell complex.⁴⁰ The NMDA-injected eyes in our OCT images also experienced thinning of the inner hyperreflective region and the outer retinal regions, which likely represented some loss of the retinal nerve fiber layer and the outer retinal layers.

However, these individual layers were not segmented in the current study because image quality was not sufficient in all scans to consistently and reliably delineate these regions.

In the occipital brain, axonal projections from the visual cortex of both hemispheres interconnect through the splenium of corpus callosum for interhemispheric transfer of visual information.⁵³⁻⁵⁷ In this study, significant FA and $\lambda_{//}$ increases in the splenium of corpus callosum occurred later than DTI changes in the optic nerve and optic tract at 4 weeks after glutamate excitotoxicity in the eye. While optic nerve injury may lead to anterograde degeneration in the visual cortex and subcortical visual nuclei at similar experimental time points,^{17,19} it remains to be elucidated whether the integrity of the splenium of corpus callosum was altered as a result of the neurodegeneration in the visual cortex after NMDA-induced injury in the visual pathway. Fractional anisotropy and/or $\lambda_{//}$ increases have been suggested to reflect white matter remodeling during neuroplasticity.^{32,58-61} There was also experimental evidence showing structural or functional reorganization mediated by the splenium of corpus callosum⁶²⁻⁶⁴ and cross-modal plasticity in the visual cortex⁶⁵⁻⁶⁷ after unilateral loss of visual input in adults. Future studies will

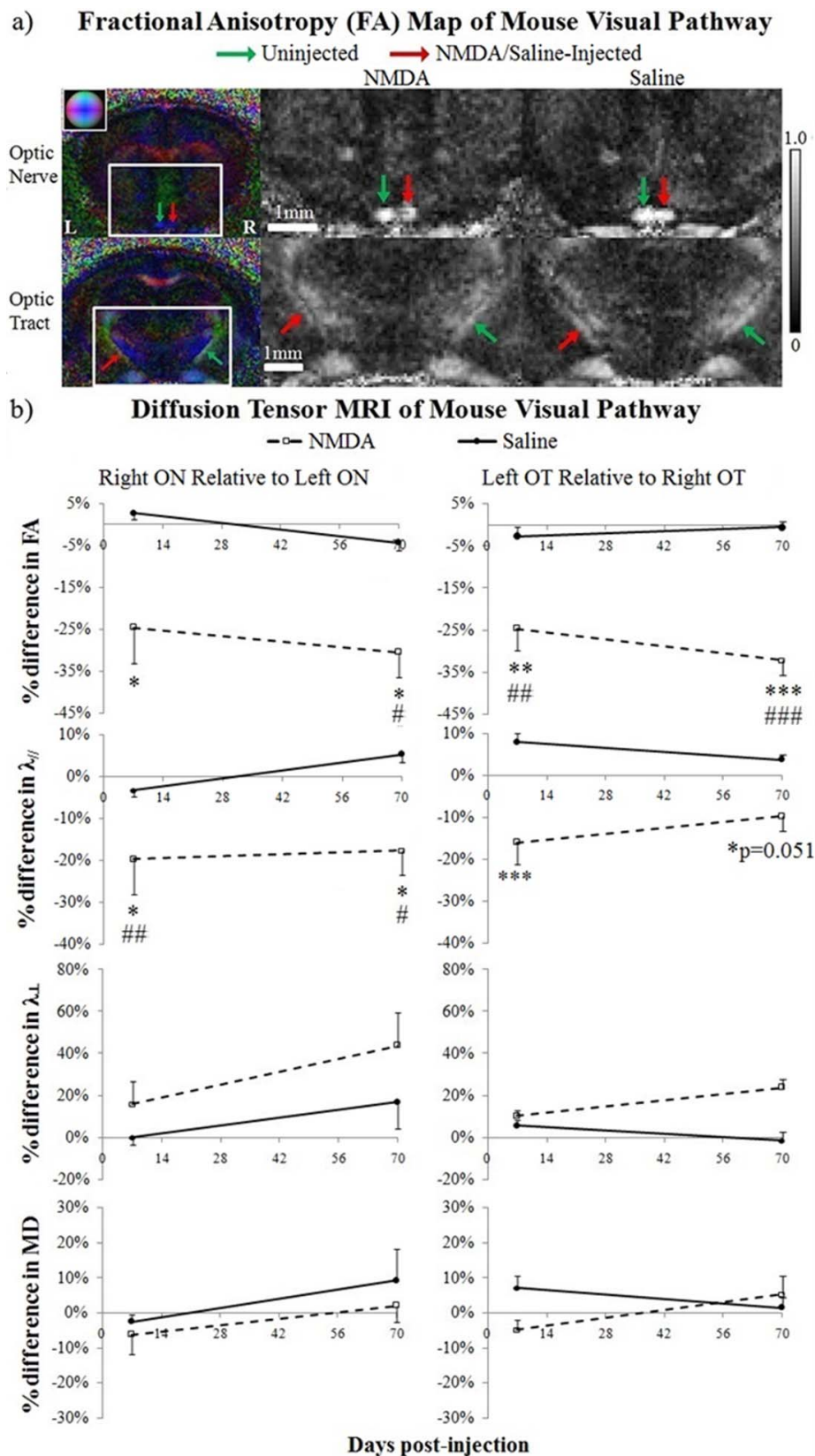
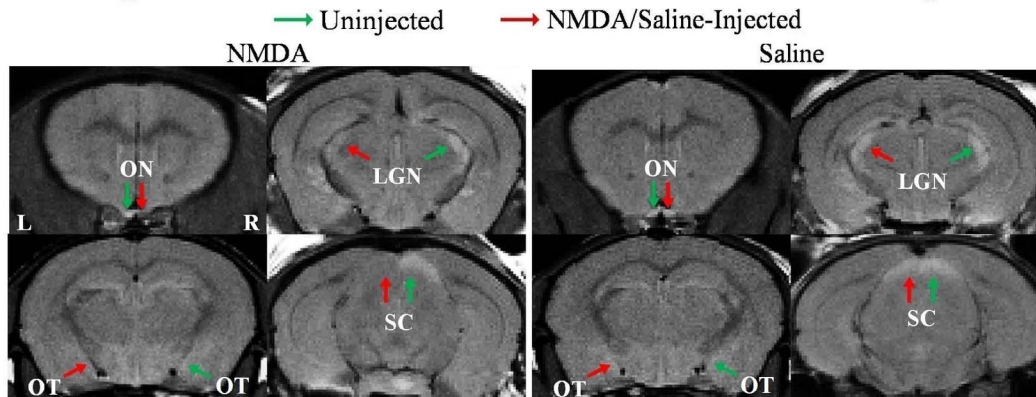


FIGURE 6. (a) *Left column:* Representative color-encoded FA directionality maps of the mouse brain at the levels of the prechiasmatic optic nerve (top) and optic tract (bottom) at 7 days post NMDA injection. *Middle and right columns:* Representative FA value maps enlarged from the white boxes in the color-encoded FA maps at 7 days after NMDA (middle column) or saline injection (right column) to the right eye. Red arrows indicate the visual pathway projected from the injected right eye. Green arrows indicate the visual pathway projected from the uninjected left eye. The grayscale bar indicates the range of FA values from 0 to 1.0. (b) Spatiotemporal DTI quantification of percentage difference (mean \pm SEM) in the right optic nerve or left optic tract relative to the left optic nerve or right optic tract at 7 and 70 days after NMDA or saline injection to the right eye

(Bonferroni's multiple comparisons tests between NMDA and saline groups, * $P < 0.05$, ** $P < 0.01$, *** $P < 0.001$; between left and right visual pathways in the NMDA group, # $P < 0.05$, ## $P < 0.01$, ### $P < 0.001$). Significantly larger FA and $\lambda_{//}$ decreases were observed in the optic nerve and optic tract of the NMDA group throughout the experimental period. No apparent difference was observed between left and right visual pathways in the saline group (color representations for the principal diffusion directions in the color-encoded FA maps: blue, caudal-rostral; red, left-right; green, dorsal-ventral).

a) T1-weighted MRI at 8 Hours after Binocular Intravitreal Mn Injection



b) Manganese-enhanced MRI Quantitation of Mouse Visual Pathway

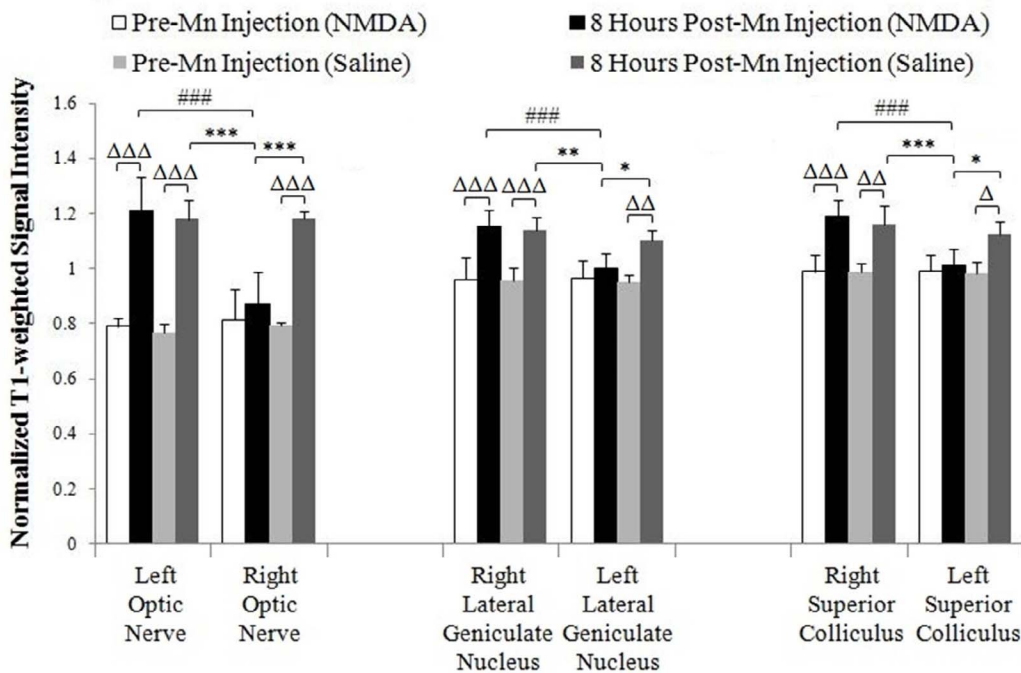


FIGURE 7. (a) T1-weighted MRIs of the mouse optic nerve (ON), optic tract (OT), lateral geniculate nucleus (LGN), and superior colliculus (SC) at 1 week after NMDA (first two columns) or saline injection (last two columns) to the right eye and 8 hours after intravitreal Mn injection to both eyes. Red arrows indicate the visual pathway projected from the NMDA- or saline-injected right eye. Green arrows indicate the visual pathway projected from the left eye without NMDA or saline injection. Manganese enhancement was observed as T1-weighted hyperintensity along the bilateral visual pathways in the saline group and in the visual pathway projected from the uninjected left eye in the NMDA group. Less apparent Mn enhancement was found along the visual pathway projected from the NMDA-injected right eye. (b) Quantitative comparisons of T1-weighted signal intensities (mean \pm SEM) of the mouse ON, LGN, and SC before (Pre-Mn) and at 8 hours after intravitreal Mn injection (post-Mn) to both eyes in the NMDA or saline group. Signal intensities were normalized to the nearby saline phantom to counter for system instability between imaging sessions. Before Mn injection, no significant difference in T1-weighted signals was observed between left and right visual pathways in either NMDA or saline group. At 8 hours post Mn injection, significant Mn enhancement was detected in the ON, LGN, and SC bilaterally in the saline group compared to pre-Mn injection. Significant Mn enhancement was also detected unilaterally along the visual pathway projected from the uninjected left eye in the NMDA group. No apparent Mn enhancement was observed along the visual pathway projected from the NMDA-injected right eye (Bonferroni's multiple comparisons tests between pre-Mn injection and 8 hours post Mn injection in the same visual pathway, $\Delta P < 0.05$, $\Delta\Delta P < 0.01$, $\Delta\Delta\Delta P < 0.001$; between NMDA and saline groups at 8 hours post Mn injection, * $P < 0.05$, ** $P < 0.01$, *** $P < 0.001$; between left and right visual pathways in the NMDA group at 8 hours post Mn injection, ### $P < 0.001$).

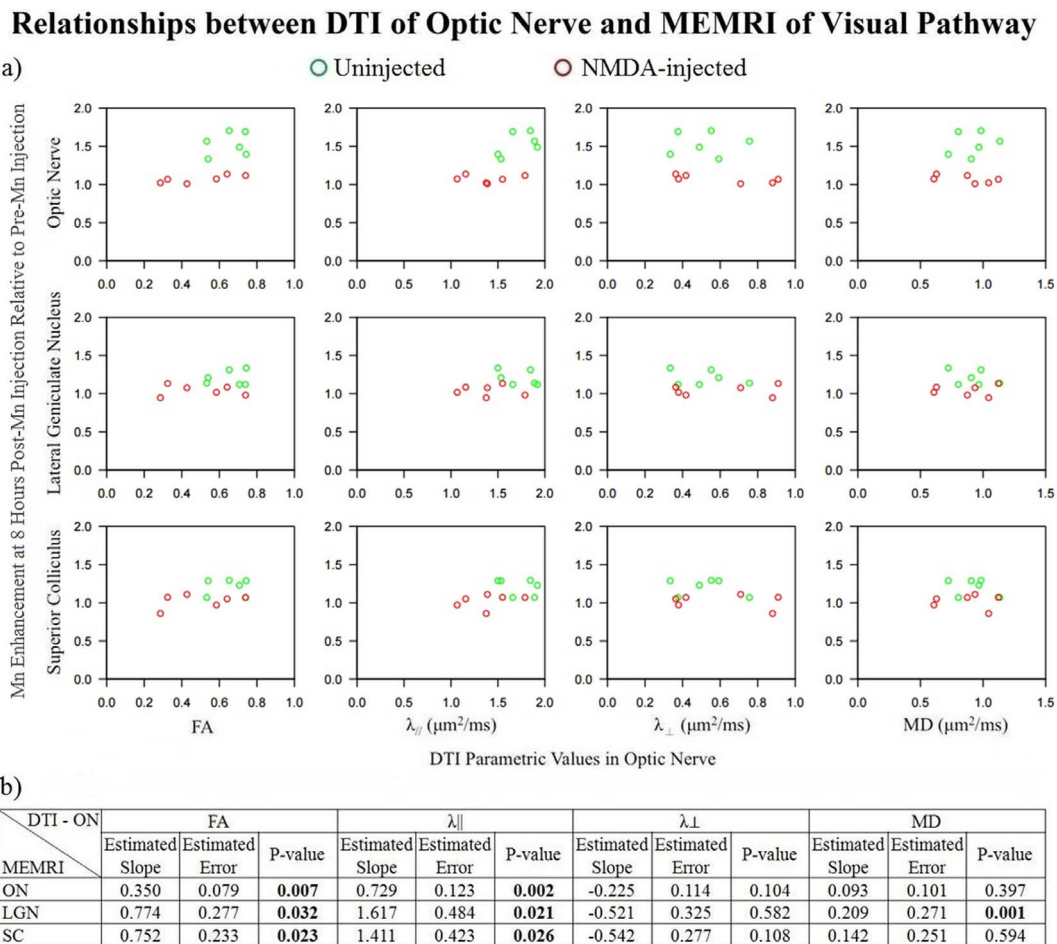


FIGURE 8. (a) Relationships between Mn enhancement (y -axis) and DTI parameters (x -axis) along bilateral visual pathways at 1 week after NMDA injection to the right mouse eye. Manganese enhancement was derived from T1-weighted signal intensities in the ON, LGN, or SC at 8 hours after binocular Mn injection relative to pre-Mn injection. Diffusion tensor MRI parameters include FA, $\lambda_{||}$, λ_{\perp} , and MD in the ON. (b) The estimated slopes of Mn signal enhancement in the ON, LGN, or SC against each DTI parameter in ON of both hemispheres at 1 week after NMDA injection to the right eye ($P < 0.05$: estimated slopes are significantly different from 0). Fractional anisotropy and $\lambda_{||}$ in the ON showed significant positive correlations with Mn enhancement in the ON, LGN, and SC.

examine how activity-induced plasticity or other neurophysiological events might be involved in the splenium of corpus callosum leading to the observed late DTI changes after excitotoxic retinal injury.

Upon intravitreal Mn injection, the exogenous Mn ions could be taken up by the retinal ganglion cells and transported anterogradely along the visual pathway to the superior colliculus and lateral geniculate nucleus.^{68,69} Since Mn is paramagnetic and can lead to hyperintensity in T1-weighted images, MEMRI is a robust technique for neuronal tract tracing and for examining anterograde transport in healthy and injured brains.^{68,70-75} Nevertheless, the relative contributions of visual pathway integrity to the Mn transport and signal enhancement along the neuronal tract have not been fully understood.⁷⁶⁻⁸⁰ In the NMDA mouse model, reduced Mn transport was observed along the NMDA-injured visual pathway after intravitreal Mn injection. However, only $\lambda_{||}$ and FA but not λ_{\perp} in the optic nerve were significantly correlated with Mn enhancement in the optic nerve, lateral geniculate nucleus, and superior colliculus. Although both axonal degeneration and demyelination had been reported in the visual pathway in the same NMDA model at similar doses and experimental time points,^{11,57} the Mn transport appeared to be preferentially susceptible to white matter integrity changes that primarily

altered water diffusion along the optic nerve in events such as microtubule and neurofilament damages as compared with the perpendicular direction in events such as myelin disruption. Because DTI may not discriminate axonal and myelin integrity specifically in the presence of other concurrent factors that may affect water diffusion such as inflammation, future studies may use more advanced diffusion MRI acquisition and modeling⁸¹⁻⁸³ to probe more specifically the structural-physiological relationships of visual pathway integrity, and the microstructural basis of Mn transport mechanisms. Future studies may also employ larger samples to investigate in more detail the relationships between MEMRI and DTI in separate injured and uninjured visual pathways. Although measuring Mn transport in the visual system using MEMRI would not be a viable option in humans at present due to the potential toxicity of MnCl_2 ,⁸⁴⁻⁸⁶ by understanding the microstructural basis of Mn transport via relating Mn enhancement to diffusion properties in the neural pathway, it may be possible to use noninvasive diffusion MR parameters such as axial diffusivity change as outcome measures to assess neuroprotective approaches targeting at axonal transport in the future. There were recent initial MEMRI studies using the relatively less toxic and Food and Drug Administration-approved Mn-chelates (e.g., Mn-DPDP) to perform neuronal tract tracing in normal rodent

optic nerves.⁸⁷ Future studies may also evaluate the potentials and safety of such Mn-chelates for assessing transport obstruction and repair in visual pathway injury compared with MnCl₂.

Intravitreal injection of NMDA can induce excitotoxic retinal injury and optic neuropathy in a dose-dependent manner.^{37,39,40} The effects of glutamate excitotoxicity on necrotic and apoptotic cell death in the retina and the brain are also dependent on the types and amount of glutamate receptors involved at the site of insult.^{16,39} As abnormalities in glutamate metabolism were suggested to play a vital role in human diseases such as retinal ischemia,⁵ glaucoma,¹¹ and diabetic retinopathy,^{12,13} the current model may hint on the mechanisms of visual pathway degeneration associated with these diseases. Future studies may refine and combine the established MRI and OCT techniques with visual psychophysical assessments⁸⁸ to evaluate the eye-brain-behavior relationships upon altering the types and degrees of excitotoxic insults mimicking different pathological conditions of human ocular diseases and injuries. It has been suggested that treatment to both the eye and the brain upon optic nerve injury may provide better outcomes than treating the eye alone.⁸⁹ Our MRI and OCT examinations of retinal loss, optic neuropathy, and corpus callosum reorganization after excitotoxic retinal injury may also provide an in vivo model system to assess the beneficial effects of different neuroprotective strategies on both the eye and the brain in future studies. Future studies may also use more advanced diffusion MRI methodology (e.g., diffusion kurtosis imaging and diffusion based spectrum imaging) to better characterize the pathophysiological events in the visual system upon ocular diseases and injuries.

CONCLUSIONS

Optical coherence tomography, DTI, and MEMRI provided an in vivo model system to monitor the spatiotemporal patterns of white matter integrity changes, the eye-brain relationships and the structural-physiological relationships in the visual system after NMDA-induced glutamate excitotoxic injury to the retina. The current results may offer in vivo imaging markers to assess the beneficial effects of neuroprotective strategies on both the anterior and posterior visual pathways upon ocular diseases and injuries in future studies. The preferential influence of reduced anterograde Mn transport by $\lambda_{//}$, but not λ_{\perp} in the neural pathway may also shed light on the microstructural basis of Mn transport mechanisms.

Acknowledgments

Supported by the National Institutes of Health P30-EY008098, R01-EY013178, T32-GM008208, and UL1-TR000005 (Bethesda, MD, USA), BrightFocus Foundation G2013077 (Clarksburg, MD, USA), Alcon Research Institute Young Investigator Grant (Fort Worth, TX, USA), Eye and Ear Foundation (Pittsburgh, PA, USA), and Research to Prevent Blindness (New York, NY, USA).

Disclosure: **L.C. Ho**, None; **B. Wang**, None; **I.P. Conner**, None; **Y. van der Merwe**, None; **R.A. Bilonick**, None; **S.-G. Kim**, None; **E.X. Wu**, None; **I.A. Sigal**, None; **G. Wollstein**, None; **J.S. Schuman**, P; **K.C. Chan**, None

References

- Lafuente MP, Villegas-Perez MP, Selles-Navarro I, Mayor-Torroglosa S, Miralles de Imperial J, Vidal-Sanz M. Retinal ganglion cell death after acute retinal ischemia is an ongoing process whose severity and duration depends on the duration of the insult. *Neuroscience*. 2002;109:157-168.
- Adachi K, Kashii S, Masai H, et al. Mechanism of the pathogenesis of glutamate neurotoxicity in retinal ischemia. *Graefes Arch Clin Exp Ophthalmol*. 1998;236:766-774.
- Joo CK, Choi JS, Ko HW, et al. Necrosis and apoptosis after retinal ischemia: involvement of NMDA-mediated excitotoxicity and p53. *Invest Ophthalmol Vis Sci*. 1999;40:713-720.
- Ishikawa M. Abnormalities in glutamate metabolism and excitotoxicity in the retinal diseases. *Scientifica*. 2013;2013:528940.
- Wakabayashi Y, Yagihashi T, Kezuka J, Muramatsu D, Usui M, Iwasaki T. Glutamate levels in aqueous humor of patients with retinal artery occlusion. *Retina*. 2006;26:432-436.
- Bien A, Seidenbecher CI, Bockers TM, Sabel BA, Kreutz MR. Apoptotic versus necrotic characteristics of retinal ganglion cell death after partial optic nerve injury. *J Neurotrauma*. 1999;16:153-163.
- Schuettauf F, Naskar R, Vorwerk CK, Zurakowski D, Dreyer EB. Ganglion cell loss after optic nerve crush mediated through AMPA-kainate and NMDA receptors. *Invest Ophthalmol Vis Sci*. 2000;41:4313-4316.
- Quigley HA, Nickells RW, Kerrigan LA, Pease ME, Thibault DJ, Zack DJ. Retinal ganglion cell death in experimental glaucoma and after axotomy occurs by apoptosis. *Invest Ophthalmol Vis Sci*. 1995;36:774-786.
- Kerrigan LA, Zack DJ, Quigley HA, Smith SD, Pease ME. TUNEL-positive ganglion cells in human primary open-angle glaucoma. *Arch Ophthalmol*. 1997;115:1031-1035.
- Okisaka S, Murakami A, Mizukawa A, Ito J. Apoptosis in retinal ganglion cell decrease in human glaucomatous eyes. *Jpn J Ophthalmol*. 1997;41:84-88.
- Naskar R, Vorwerk CK, Dreyer EB. Concurrent downregulation of a glutamate transporter and receptor in glaucoma. *Invest Ophthalmol Vis Sci*. 2000;41:1940-1944.
- Hernandez C, Simo R. Neuroprotection in diabetic retinopathy. *Curr Diabetes Rep*. 2012;12:329-337.
- Ambati J, Chalam KV, Chawla DK, et al. Elevated gamma-aminobutyric acid, glutamate, and vascular endothelial growth factor levels in the vitreous of patients with proliferative diabetic retinopathy. *Arch Ophthalmol*. 1997;115:1161-1166.
- Seitz R, Tamm ER. N-methyl-D-aspartate (NMDA)-mediated excitotoxic damage: a mouse model of acute retinal ganglion cell damage. *Methods Mol Biol*. 2013;935:99-109.
- Zhang J, Diamond JS. Distinct perisynaptic and synaptic localization of NMDA and AMPA receptors on ganglion cells in rat retina. *J Comp Neurosci*. 2006;498:810-820.
- Saggu SK, Chotaliya HP, Blumbergs PC, Casson RJ. Wallerian-like axonal degeneration in the optic nerve after excitotoxic retinal insult: an ultrastructural study. *BMC Neurosci*. 2010;11:97.
- Liu Y, McDowell CM, Zhang Z, Tebow HE, Wordinger RJ, Clark AF. Monitoring retinal morphologic and functional changes in mice following optic nerve crush. *Invest Ophthalmol Vis Sci*. 2014;55:3766-3774.
- Yucel YH, Zhang Q, Weinreb RN, Kaufman PL, Gupta N. Effects of retinal ganglion cell loss on magno-, parvo-, koniocellular pathways in the lateral geniculate nucleus and visual cortex in glaucoma. *Progr Retin Eye Res*. 2003;22:465-481.
- You Y, Gupta VK, Graham SL, Klistorner A. Anterograde degeneration along the visual pathway after optic nerve injury. *PLoS One*. 2012;7:e52061.
- Toosy AT, Ciccarelli O, Parker GJ, Wheeler-Kingshott CA, Miller DH, Thompson AJ. Characterizing function-structure relationships in the human visual system with functional MRI and diffusion tensor imaging. *Neuroimage*. 2004;21:1452-1463.

21. Berkowitz BA. MRI of retinal and optic nerve physiology. *NMR Biomed.* 2008;21:927.
22. Shih YY, Muir ER, Li G, De La Garza BH, Duong TQ. High-resolution 3D MR microangiography of the rat ocular circulation. *Radiology.* 2012;264:234-241.
23. Ho LC, Conner IP, Do CW, et al. In vivo assessment of aqueous humor dynamics upon chronic ocular hypertension and hypotensive drug treatment using gadolinium-enhanced MRI. *Invest Ophthalmol Vis Sci.* 2014;55:3747-3757.
24. Ho LC, Sigal IA, Jan NJ, et al. Magic angle-enhanced MRI of fibrous microstructures in sclera and cornea with and without intraocular pressure loading. *Invest Ophthalmol Vis Sci.* 2014;55:5662-5672.
25. Chan KC, So KF, Wu EX. Proton magnetic resonance spectroscopy revealed choline reduction in the visual cortex in an experimental model of chronic glaucoma. *Exp Eye Res.* 2009;88:65-70.
26. Dijkhuizen RM, van Lookeren Campagne M, Niendorf T, et al. Status of the neonatal rat brain after NMDA-induced excitotoxic injury as measured by MRI, MRS and metabolic imaging. *NMR Biomed.* 1996;9:84-92.
27. Van Lookeren Campagne M, Verheul HB, Vermeulen JP, Balazs R, Boer GJ, Nicolay K. Developmental changes in NMDA-induced cell swelling and its transition to necrosis measured with 1H magnetic resonance imaging, impedance and histology. *Brain Res Dev Brain Res.* 1996;93:109-119.
28. Lee J, Kim SW, Lee SC, Kwon OW, Kim YD, Byeon SH. Co-occurrence of acute retinal artery occlusion and acute ischemic stroke: diffusion-weighted magnetic resonance imaging study. *Am J Ophthalmol.* 2014;157:1231-1238.
29. Al-Shafai LS, Mikulis DJ. Diffusion MR imaging in a case of acute ischemic optic neuropathy. *AJNR Am J Neuroradiol.* 2006;27:255-257.
30. Sun SW, Liang HF, Cross AH, Song SK. Evolving Wallerian degeneration after transient retinal ischemia in mice characterized by diffusion tensor imaging. *Neuroimage.* 2008;40:1-10.
31. Song SK, Sun SW, Ju WK, Lin SJ, Cross AH, Neufeld AH. Diffusion tensor imaging detects and differentiates axon and myelin degeneration in mouse optic nerve after retinal ischemia. *Neuroimage.* 2003;20:1714-1722.
32. Chan KC, Cheng JS, Fan S, Zhou IY, Yang J, Wu EX. In vivo evaluation of retinal and callosal projections in early postnatal development and plasticity using manganese-enhanced MRI and diffusion tensor imaging. *Neuroimage.* 2012;59:2274-2283.
33. Chan KC, Khong PL, Lau HF, Cheung PT, Wu EX. Late measures of microstructural alterations in severe neonatal hypoxic-ischemic encephalopathy by MR diffusion tensor imaging. *Int J Dev Neurosci.* 2009;27:607-615.
34. Chan KC, Xing KK, Cheung MM, Zhou IY, Wu EX. Functional MRI of postnatal visual development in normal and hypoxic-ischemic-injured superior colliculi. *Neuroimage.* 2010;49:2013-2020.
35. Chan KC, Kancherla S, Fan SJ, Wu EX. Long-term effects of neonatal hypoxia-ischemia on structural and physiological integrity of the eye and visual pathway by multimodal MRI. *Invest Ophthalmol Vis Sci.* 2015;56:1-9.
36. Horsfield MA, Jones DK. Applications of diffusion-weighted and diffusion tensor MRI to white matter diseases - a review. *NMR Biomed.* 2002;15:570-577.
37. Lam TT, Ablner AS, Kwong JM, Tso MO. N-methyl-D-aspartate (NMDA)-induced apoptosis in rat retina. *Invest Ophthalmol Vis Sci.* 1999;40:2391-2397.
38. Honjo M, Tanihara H, Kido N, Inatani M, Okazaki K, Honda Y. Expression of ciliary neurotrophic factor activated by retinal Muller cells in eyes with NMDA- and kainic acid-induced neuronal death. *Invest Ophthalmol Vis Sci.* 2000;41:552-560.
39. Ientile R, Macaione V, Teletta M, Pedale S, Torre V, Macaione S. Apoptosis and necrosis occurring in excitotoxic cell death in isolated chick embryo retina. *J Neurochem.* 2001;79:71-78.
40. Nakano N, Ikeda HO, Hangai M, et al. Longitudinal and simultaneous imaging of retinal ganglion cells and inner retinal layers in a mouse model of glaucoma induced by N-methyl-D-aspartate. *Invest Ophthalmol Vis Sci.* 2011;52:8754-8762.
41. Paxinos G, Watson C. *The Rat Brain in Stereotaxic Coordinates: Hard Cover Edition.* New Delhi, India: Elsevier Science; 2006.
42. Paxinos G, Franklin KBJ. *The Mouse Brain in Stereotaxic Coordinates.* Waltham, MA: Elsevier Academic Press; 2004.
43. Gabriele ML, Ishikawa H, Schuman JS, et al. Optic nerve crush mice followed longitudinally with spectral domain optical coherence tomography. *Invest Ophthalmol Vis Sci.* 2011;52:2250-2254.
44. Galindo-Romero C, Valiente-Soriano FJ, Jimenez-Lopez M, et al. Effect of brain-derived neurotrophic factor on mouse axotomized retinal ganglion cells and phagocytic microglia. *Invest Ophthalmol Vis Sci.* 2013;54:974-985.
45. Kerr NM, Johnson CS, Zhang J, Eady EK, Green CR, Danesh-Meyer HV. High pressure-induced retinal ischaemia reperfusion causes upregulation of gap junction protein connexin43 prior to retinal ganglion cell loss. *Exp Neurol.* 2012;234:144-152.
46. Macharadze T, Goldschmidt J, Marunde M, et al. Interretinal transduction of injury signals after unilateral optic nerve crush. *Neuroreport.* 2009;20:301-305.
47. Panagis L, Thanos S, Fischer D, Dermon CR. Unilateral optic nerve crush induces bilateral retinal glial cell proliferation. *Eur J Neurosci.* 2005;21:2305-2309.
48. Forrester J, Peters A. Nerve fibres in optic nerve of rat. *Nature.* 1967;214:245-247.
49. Kim JH, Budde MD, Liang HF, et al. Detecting axon damage in spinal cord from a mouse model of multiple sclerosis. *Neurobiol Dis.* 2006;21:626-632.
50. Song SK, Sun SW, Ramsbottom MJ, Chang C, Russell J, Cross AH. Dysmyelination revealed through MRI as increased radial (but unchanged axial) diffusion of water. *Neuroimage.* 2002;17:1429-1436.
51. Song SK, Yoshino J, Le TQ, et al. Demyelination increases radial diffusivity in corpus callosum of mouse brain. *Neuroimage.* 2005;26:132-140.
52. Thomalla G, Glauche V, Koch MA, Beaulieu C, Weiller C, Rother J. Diffusion tensor imaging detects early Wallerian degeneration of the pyramidal tract after ischemic stroke. *Neuroimage.* 2004;22:1767-1774.
53. Martinez-Garcia F, Gonzalez-Hernandez T, Martinez-Millan L. Pyramidal and nonpyramidal callosal cells in the striate cortex of the adult rat. *J Comp Neurosci.* 1994;350:439-451.
54. Cusick CG, Lund RD. The distribution of the callosal projection to the occipital visual cortex in rats and mice. *Brain Res.* 1981;214:239-259.
55. Montero VM. Retinotopy of cortical connections between the striate cortex and extrastriate visual areas in the rat. *Exp Brain Res.* 1993;94:1-15.
56. Chan KC, Fan SJ, Chan RW, Cheng JS, Zhou IY, Wu EX. In vivo visuotopic brain mapping with manganese-enhanced MRI and resting-state functional connectivity MRI. *Neuroimage.* 2014;90:235-245.
57. Knyazeva MG. Splenium of corpus callosum: patterns of interhemispheric interaction in children and adults. *Neural Plast.* 2013;2013:639430.

58. Mackey AP, Whitaker KJ, Bunge SA. Experience-dependent plasticity in white matter microstructure: reasoning training alters structural connectivity. *Front Neuroanat.* 2012;6:32.
59. Scholz J, Klein MC, Behrens TE, Johansen-Berg H. Training induces changes in white-matter architecture. *Nat Neurosci.* 2009;12:1370-1371.
60. Zatorre RJ, Fields RD, Johansen-Berg H. Plasticity in gray and white: neuroimaging changes in brain structure during learning. *Nat Neurosci.* 2012;15:528-536.
61. Ding G, Jiang Q, Li L, et al. Magnetic resonance imaging investigation of axonal remodeling and angiogenesis after embolic stroke in sildenafil-treated rats. *J Cereb Blood Flow Metabolism.* 2008;28:1440-1448.
62. Shi J, Collignon O, Xu L, et al. Impact of early and late visual deprivation on the structure of the corpus callosum: a study combining thickness profile with surface tensor-based morphometry [published online ahead of print February 4, 2015]. *Neuroinformatics.* doi:10.1007/s12021-014-9259-9.
63. Noppeney U, Friston KJ, Ashburner J, Frackowiak R, Price CJ. Early visual deprivation induces structural plasticity in gray and white matter. *Curr Biol.* 2005;15:R488-R490.
64. Pietrasanta M, Restani L, Caleo M. The corpus callosum and the visual cortex: plasticity is a game for two. *Neural Plast.* 2012;2012:838672.
65. Zaidel E, Iacoboni M. *The Parallel Brain: The Cognitive Neuroscience of the Corpus Callosum.* Cambridge, MA: MIT Press; 2003.
66. Sugita Y. Global plasticity in adult visual cortex following reversal of visual input. *Nature.* 1996;380:523-526.
67. Van Brussel L, Gerits A, Arckens L. Evidence for cross-modal plasticity in adult mouse visual cortex following monocular enucleation. *Cereb Cortex.* 2011;21:2133-2146.
68. Chan KC, Fu QL, Hui ES, So KF, Wu EX. Evaluation of the retina and optic nerve in a rat model of chronic glaucoma using in vivo manganese-enhanced magnetic resonance imaging. *Neuroimage.* 2008;40:1166-1174.
69. Chan KC, Li J, Kau P, et al. In vivo retinotopic mapping of superior colliculus using manganese-enhanced magnetic resonance imaging. *Neuroimage.* 2011;54:389-395.
70. Pautler RG, Silva AC, Koretsky AP. In vivo neuronal tract tracing using manganese-enhanced magnetic resonance imaging. *Magn Reson Med.* 1998;40:740-748.
71. Pautler RG. In vivo, trans-synaptic tract-tracing utilizing manganese-enhanced magnetic resonance imaging (MEMRI). *NMR Biomed.* 2004;17:595-601.
72. Ryu S, Brown SL, Kolozsvary A, Ewing JR, Kim JH. Noninvasive detection of radiation-induced optic neuropathy by manganese-enhanced MRI. *Radiat Res.* 2002;157:500-505.
73. Thuen M, Singstad TE, Pedersen TB, et al. Manganese-enhanced MRI of the optic visual pathway and optic nerve injury in adult rats. *J Magn Reson Imaging.* 2005;22:492-500.
74. Sun S-W, Campbell B, Lunderville C, Won E, Liang H-F. Noninvasive topical loading for manganese-enhanced MRI of the mouse visual system. *Invest Ophthalmol Vis Sci.* 2011;52:3914-3920.
75. Liang Y-X, Cheung SW, Chan KC, Wu EX, Tay DK, Ellis-Behnke RG. CNS regeneration after chronic injury using a self-assembled nanomaterial and MEMRI for real-time in vivo monitoring. *Nanomedicine.* 2011;7:351-359.
76. Aschner M, Gannon M, Kimelberg HK. Manganese uptake and efflux in cultured rat astrocytes. *J Neurochem.* 1992;58:730-735.
77. Slood WN, Gramsbergen JB. Axonal transport of manganese and its relevance to selective neurotoxicity in the rat basal ganglia. *Brain Res.* 1994;657:124-132.
78. Bearer EL, Falzone TL, Zhang X, Biris O, Rasin A, Jacobs RE. Role of neuronal activity and kinesin on tract tracing by manganese-enhanced MRI (MEMRI). *Neuroimage.* 2007;37(suppl 1):S37-S46.
79. Lowe AS, Thompson ID, Sibson NR. Quantitative manganese tract tracing: dose-dependent and activity-independent terminal labelling in the mouse visual system. *NMR Biomed.* 2008;21:859-867.
80. Thuen M, Berry M, Pedersen TB, et al. Manganese-enhanced MRI of the rat visual pathway: acute neural toxicity, contrast enhancement, axon resolution, axonal transport, and clearance of Mn(2+). *J Magn Reson Imaging.* 2008;28:855-865.
81. Hui ES, Cheung MM, Chan KC, Wu EX. B-value dependence of DTI quantitation and sensitivity in detecting neural tissue changes. *Neuroimage.* 2010;49:2366-2374.
82. Wang Y, Sun P, Wang Q, et al. Differentiation and quantification of inflammation, demyelination and axon injury or loss in multiple sclerosis. *Brain.* 2015;138(pt 5):1223-1238.
83. Cheung MM, Hui ES, Chan KC, Helpert JA, Qi L, Wu EX. Does diffusion kurtosis imaging lead to better neural tissue characterization? A rodent brain maturation study. *Neuroimage.* 2009;45:386-392.
84. Luo L, Xu H, Li Y, et al. Manganese-enhanced MRI optic nerve tracking: effect of intravitreal manganese dose on retinal toxicity. *NMR Biomed.* 2012;25:1360-1368.
85. Lindsey JD, Grob SR, Scadeng M, Duong-Polk K, Weinreb RN. Ocular integrity following manganese labeling of the visual system for MRI. *Magn Reson Imaging.* 2013;31:865-874.
86. Lin T-H, Chiang C-W, Trinkaus K, et al. (MEMRI) via topical loading of Mn2+ significantly impairs mouse visual acuity: a comparison with intravitreal injection. *NMR Biomed.* 2014;27:390-398.
87. Olsen O, Thuen M, Berry M, et al. Axon tracing in the adult rat optic nerve and tract after intravitreal injection of MnDPDP using a semiautomatic segmentation technique. *J Magn Reson Imaging.* 2008;27:34-42.
88. Prusky GT, Alam NM, Beekman S, Douglas RM. Rapid quantification of adult and developing mouse spatial vision using a virtual optomotor system. *Invest Ophthalmol Vis Sci.* 2004;45:4611-4616.
89. Weber AJ, Viswanathan S, Ramanathan C, Harman CD. Combined application of BDNF to the eye and brain enhances ganglion cell survival and function in the cat after optic nerve injury. *Invest Ophthalmol Vis Sci.* 2010;51:327-334.